

Two energy scales in the spin excitations of the high-temperature superconductor $\text{La}_{2-x}\text{Sr}_x\text{CuO}_4$

B. VIGNOLLE¹, S. M. HAYDEN^{1*}, D. F. McMORROW^{2,3}, H. M. RØNNOW⁴, B. LAKE⁵, C. D. FROST³ AND T. G. PERRING³

¹H. H. Wills Physics Laboratory, University of Bristol, Tyndall Ave., Bristol BS8 1TL, UK

²London Centre for Nanotechnology and Department of Physics and Astronomy, University College London, London WC1E 6BT, UK

³ISIS Facility, Rutherford Appleton Laboratory, Chilton, Didcot OX11 0QX, UK

⁴Laboratory for Neutron Scattering, ETH-Zürich and Paul Scherrer Institut, 5232 Villigen, Switzerland

⁵Hahn-Meitner Institut, Berlin D-14109, Germany

*e-mail: s.hayden@bris.ac.uk

Published online: 18 February 2007; doi:10.1038/nphys546

The excitations responsible for producing high-temperature superconductivity in the copper oxides have yet to be identified. Two promising candidates are collective spin excitations and phonons¹. A recent argument against spin excitations is based on their inability to explain structures observed in electronic spectroscopies such as photoemission^{2–5} and optical conductivity^{6,7}. Here, we use inelastic neutron scattering to demonstrate that collective spin excitations in optimally doped $\text{La}_{2-x}\text{Sr}_x\text{CuO}_4$ are more structured than previously thought. The excitations have a two-component structure with a low-frequency component strongest around 18 meV and a broader component peaking near 40–70 meV. The second component carries most of the spectral weight and its energy matches structures observed in photoemission^{2–5} in the range 50–90 meV. Our results demonstrate that collective spin excitations can explain features of electronic spectroscopies and are therefore likely to be strongly coupled to the electron quasiparticles.

Since their discovery, considerable progress has been made in understanding the properties of the high-critical-temperature, T_c , cuprate superconductors. We know, for example, that the superconductivity involves Cooper pairs, but with d -wave rather than the s -wave pairing of conventional Bardeen–Cooper–Schrieffer (BCS) superconductors. One outstanding issue is the pairing mechanism itself. For conventional superconductors, identifying the bosonic excitations that strongly couple to the electron quasiparticles played a pivotal role in confirming the phonon-mediated pairing mechanism^{8,9}. In the case of the copper oxide superconductors, electronic spectroscopies such as angle-resolved photoemission (ARPES) and infrared optical conductivity measurements^{6,7} have revealed structures in the low-energy electronic excitations, which may reflect coupling to bosonic excitations. ARPES measurements on $\text{Bi}_2\text{Sr}_2\text{CaCu}_2\text{O}_8$, $\text{Bi}_2\text{Sr}_2\text{CuO}_6$ and $\text{La}_{2-x}\text{Sr}_x\text{CuO}_4$ have shown rapid changes or ‘kinks’ in the quasiparticle dispersion, $E(k)$, for energies in the range 50–80 meV (refs 2–5). These features in ARPES have been interpreted in terms of coupling to phonon modes⁵. However, the ARPES measurements do not distinguish between coupling to lattice and spin excitations. Identifying phonons as the strongly coupled bosons is not without

its difficulties: we must explain what is special about the phonons in the cuprates; interactions with phonons do not naturally explain other important properties of the cuprates, such as the large linear temperature dependence of the normal-state resistivity at optimal doping and the origin of d -wave symmetry of the superconducting gap itself.

The interpretation of the kinks and other features in electronic spectroscopies^{2–7} in terms of coupling to collective spin excitations¹⁰ has been hampered by the lack of magnetic spectroscopy data. Most neutron scattering data refer to $\text{YBa}_2\text{Cu}_3\text{O}_{6+x}$, a compound for which ARPES data are scarce. Although ARPES kinks have also been reported in $\text{La}_{2-x}\text{Sr}_x\text{CuO}_4$, comparison with neutron scattering is restricted by the fact that high-resolution studies in this compound have only been made for energies below the relevant 50–80 meV energy window^{11–14}. At these and higher energies of relevance, only coarsely averaged data are available¹⁵, precluding a detailed comparison with electronic spectroscopies. Here, we report a high-resolution neutron scattering study of the magnetic excitations in optimally doped $\text{La}_{2-x}\text{Sr}_x\text{CuO}_4$ ($x = 0.16$, $T_c = 38.5$ K) designed to fill this gap in our knowledge. For our experiments, we have grown new single crystals by a floating-zone technique and assembled a sample with a total mass of 48.5 g (see the Supplementary Information). The experiments were carried out using the MAPS spectrometer at the ISIS spallation neutron source, Rutherford–Appleton Laboratory. MAPS has an order of magnitude better momentum resolution than the MARI instrument used for the previous high-energy study¹⁵.

The parent compound La_2CuO_4 of the $\text{La}_{2-x}\text{Sr}_x\text{CuO}_4$ superconducting series exhibits antiferromagnetic order with an ordering wavevector of $\mathbf{Q}_{2D} = (1/2, 1/2)$. Doping induces superconductivity and causes low-frequency incommensurate fluctuations^{11,12} to develop with wavevectors $\mathbf{Q}_{2D} = (1/2, 1/2 \pm \delta)$ and $(1/2 \pm \delta, 1/2)$. These excitations broaden¹³ and disperse inwards initially towards $(1/2, 1/2)$ (ref. 14) with increasing energy.

Neutron spectroscopy provides a direct probe of the magnetic response function $\chi''(\mathbf{Q}, \omega)$. Figure 1a–h shows wavevector-dependent images of the magnetic response at various energies demonstrating how it evolves with energy. At low energies,

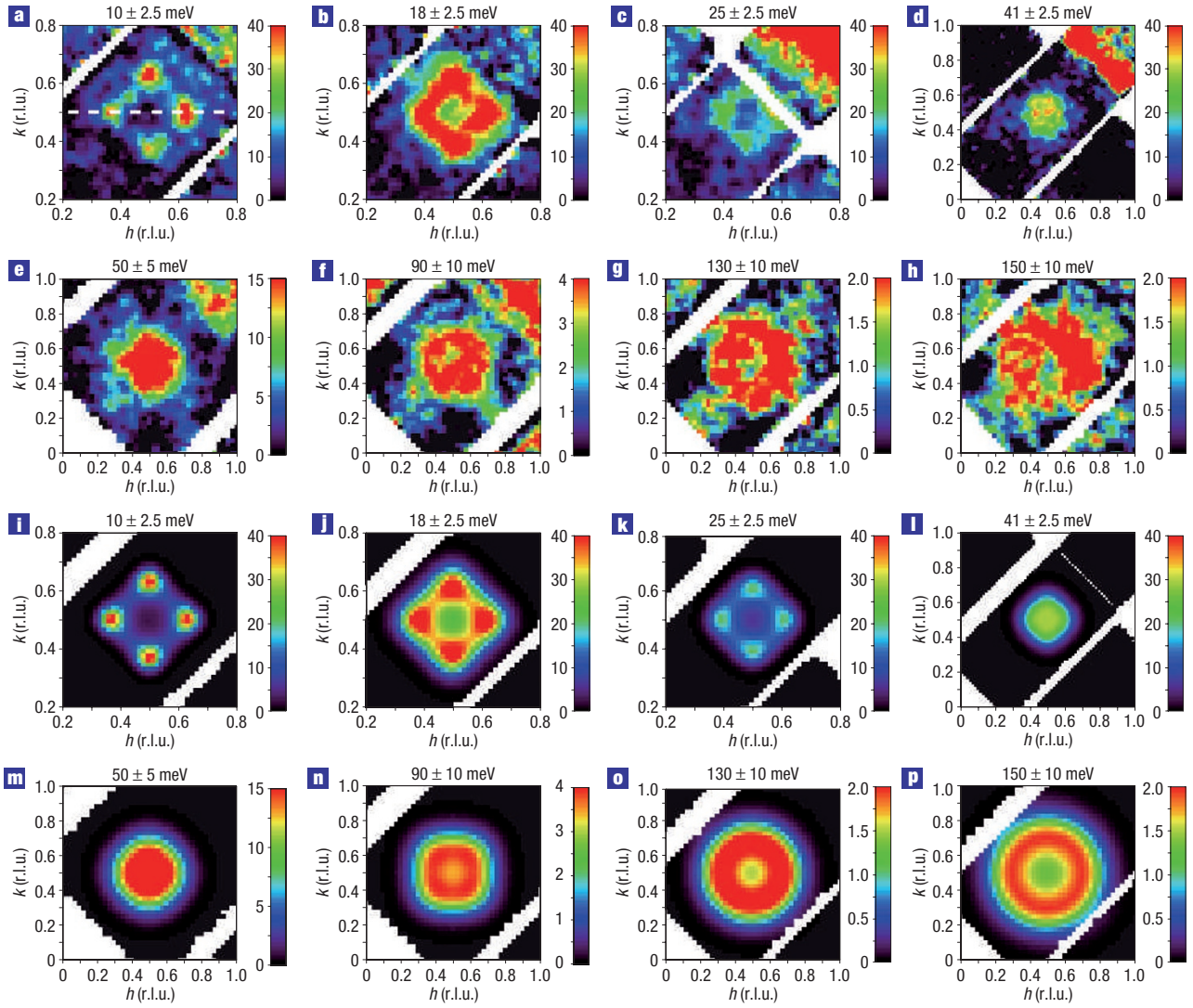


Figure 1 Images of the magnetic excitations in $\text{La}_{1.84}\text{Sr}_{0.16}\text{CuO}_4$. **a–h**, The measured $\chi''(\mathbf{Q}, \omega)$ is plotted in units of $\mu_B^2 \text{eV}^{-1} \text{f.u.}^{-1}$ as a function of wavevector for various energies in the superconducting phase at $T = 12 \text{K}$. **a–c**, The emergence and disappearance of the component at $(1/2 \pm \delta, 1/2)$ and $(1/2, 1/2 \pm \delta)$, which is most intense at lower energies. **d–h**, The higher-energy component, which emerges around 41 meV and disperses outwards with increasing energy. **i–p**, Model fits to the images of the magnetic excitations shown in **a–h**. The phenomenological model (equation (1)) provides a good description of the experimentally measured magnetic excitations and can therefore be used to parameterize the data. At higher energies (**n–p**), the data are best fitted with the model $\chi''(\mathbf{Q}, \omega)$ rotated 45° in the h – k plane. The anisotropy is strongest for panel **n**. Wavevectors are labelled by their positions in reciprocal space $\mathbf{Q} = h\mathbf{a}^* + k\mathbf{b}^* + l\mathbf{c}^*$. A background of the form $\alpha + \beta|\mathbf{Q}|^2$ has been subtracted from the data before conversion to $\chi''(\mathbf{Q}, \omega)$.

$E = 10 \text{ meV}$ (Fig. 1a), we observe the low-energy incommensurate excitations^{11–14}. As the energy is increased, $E = 18 \text{ meV}$ (Fig. 1b), the response becomes stronger, the pattern fills in along the line connecting the nearest-neighbour incommensurate peaks and the incommensurability δ decreases. For $E = 25 \text{ meV}$ (Fig. 1c), the intensity of the pattern is noticeably attenuated. On further increasing to $E = 41 \text{ meV}$ (Fig. 1d), the response ‘recovers’, becoming more intense again, but is now peaked at the commensurate wavevector $(1/2, 1/2)$. At higher energy $E = 90 \text{ meV}$ (Fig. 1f), the structure resembles a square box with the corners pointing along the (110) -type directions, that is, towards the Brillouin zone centre. Thus, the square pattern is rotated 45° with respect to the low-energy response (for example, Fig. 1b). A similar high-energy response has been observed in underdoped

$\text{YBa}_2\text{Cu}_3\text{O}_{6+x}$ (refs 16,17) and the stripe-ordered composition $\text{La}_{1.875}\text{Ba}_{0.125}\text{CuO}_4$ (ref. 18). Thus, a rotated continuum seems to be a universal feature of the cuprates.

To make our analysis quantitative, we fitted a modified lorentzian cross-section previously used to describe the cuprates and other systems¹⁹ to the data:

$$\chi''(\mathbf{Q}, \omega) = \chi_s(\omega) \frac{\kappa^4(\omega)}{[\kappa^2(\omega) + R(\mathbf{Q})]^2} \quad (1)$$

with

$$R(\mathbf{Q}) = \frac{[(h - \frac{1}{2})^2 + (k - \frac{1}{2})^2 - \delta^2]^2 + \lambda(h - \frac{1}{2})^2(k - \frac{1}{2})^2}{4\delta^2}$$

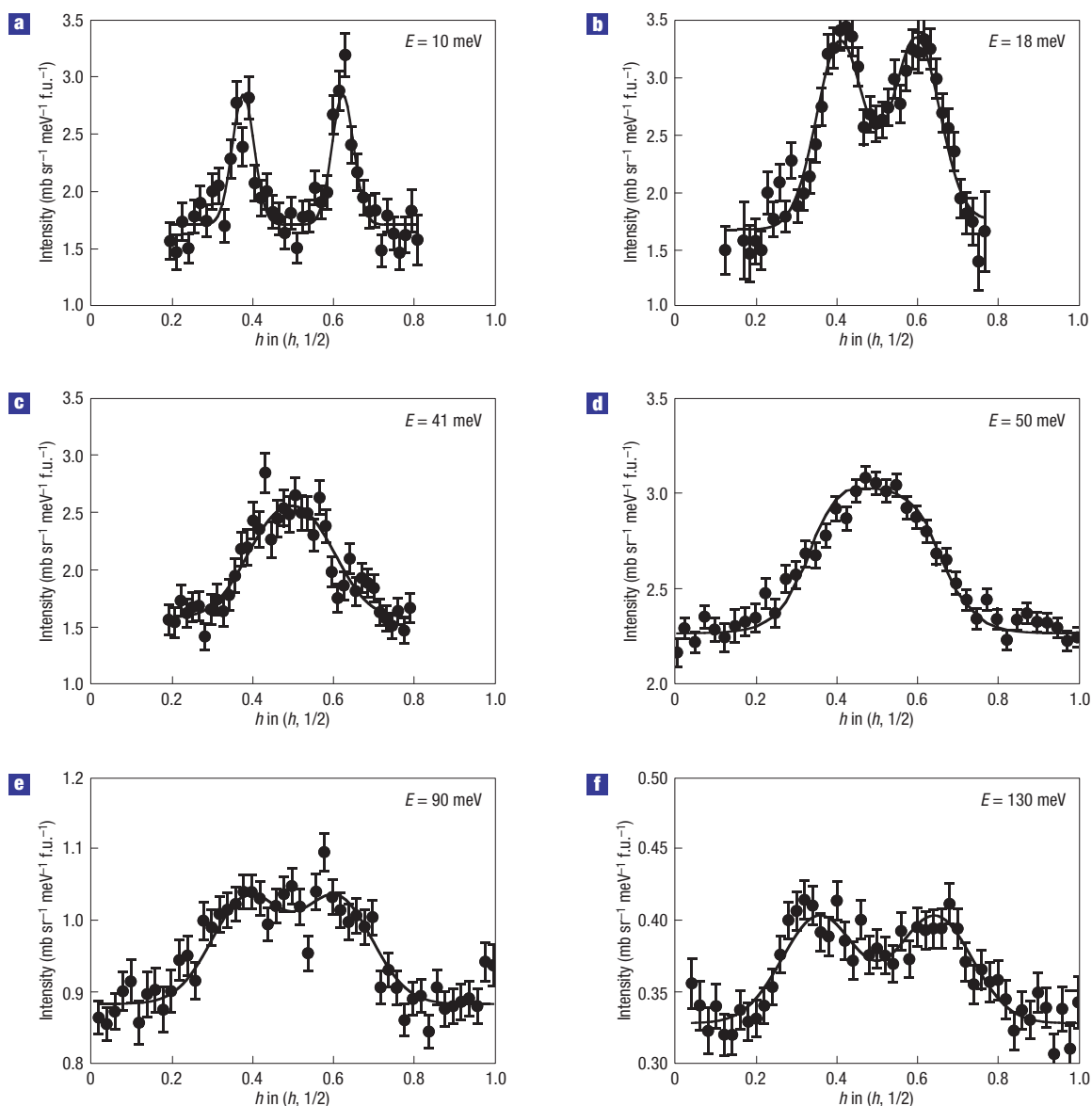


Figure 2 Magnetic excitations in $\text{La}_{1.84}\text{Sr}_{0.16}\text{CuO}_4$. **a–f**, The variation of the scattered intensity with wavevector for various fixed excitation energies at $T = 12$ K. The trajectory of the cut is shown by the dashed line in Fig. 1a. **a** and **b** show the incommensurate low-frequency component of the response. The high-frequency component is strongest for 40–50 meV (**c–f**). Two distinct peaks are seen at higher energies (**e, f**), these disperse away from $(1/2, 1/2)$ in a similar manner to the spin-wave excitations in the parent compound La_2CuO_4 . The error bars are determined from the number of neutrons counted.

where $\kappa(\omega)$ is an inverse correlation length, the position of the four peaks is specified by δ , and λ controls the shape of the pattern ($\lambda = 4$ corresponds to four distinct peaks and $\lambda = 0$ corresponds to a pattern with circular symmetry). Further details of the experimental method and analysis are given in the Supplementary Information.

Figure 1i–p shows plots of the fitted model response for the same energies as Fig. 1a–h. Another way of displaying the results is to take constant energy cuts through our data set. Figure 2 shows cuts along the dashed trajectory in Fig. 1 for various energies together with fits of our model response (equation (1)) convolved with the experimental resolution. The good agreement between the data and fits allows us to use the parameters derived from the fits (Fig. 3) to interpret our results. To distinguish between

magnetic and phonon scattering, the experiment was carried out at a number of incident energies. This means that the same in-plane momentum (h, k) could be probed with a variety of l (momentum perpendicular to plane) values and strong phonons isolated. The fact that data collected with different incident energies yield similar results confirms the validity of our analysis. We have expressed the strength of the spin fluctuations in terms of the local or wavevector-averaged susceptibility $\chi''(\omega) = \int \chi''(\mathbf{Q}, \omega) d^3Q / \int d^3Q$ determined from the fitted cross-section. The local susceptibility, $\chi''(\omega)$, is a measure of the density of magnetic excitations for a given energy.

Figure 3a shows one of the key results of this work: the magnetic response of $\text{La}_{1.84}\text{Sr}_{0.16}\text{CuO}_4$ has a two-component structure. The lower-energy peak corresponds to the incommensurate structure that is rapidly attenuated above 20 meV. The

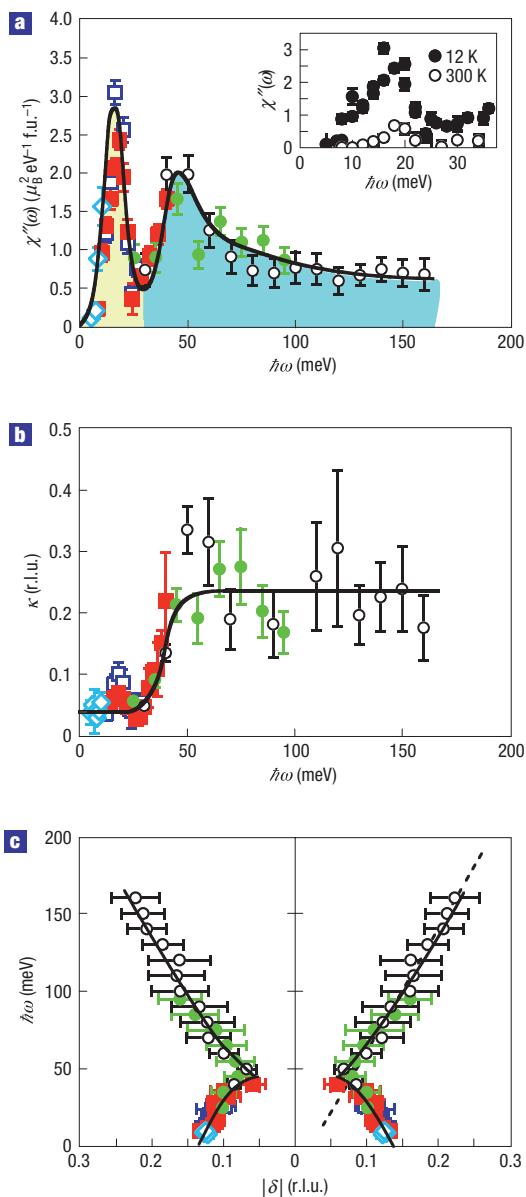


Figure 3 Magnetic excitation spectrum and evolution of the form of the magnetic response with energy. **a**, The wavevector-averaged susceptibility, $\chi''(\omega)$, shows a 'peak-dip-hump' structure suggesting that the magnetic response has two components. **b**, The emergence of the higher-frequency component above about 40 meV corresponds to a broadening of the response in the wavevector as demonstrated by the rapid increase in κ . **c**, There is a strong dispersion of the peak positions in constant excitation-energy cuts as shown by the energy dependence of the incommensurability $\delta(\omega)$. The high-energy dispersion indicates the persistence of residual antiferromagnetic interactions. The symbols in the main panels indicate different incident energies: $E_i = 30$ (diamond), 55 (open square), 90 (filled square), 160 (filled circle), 240 meV (open circle). The inset in **a** shows that the low-energy peak is strongly suppressed at $T = 300$ K confirming that it is mostly magnetic in origin. The error bars are statistically determined from least-squares fitting.

higher-energy structure is peaked at $(1/2, 1/2)$ for $E \approx 40$ –50 meV and broadens out with increasing energy above this. Although the wavevector-averaged susceptibility, $\chi''(\omega)$, of the higher-frequency component is peaked around 50 meV, it has a

long tail with a measurable response at the highest energies probed ($E = 155$ meV) in this experiment.

It is interesting to compare the present results with those obtained on $\text{La}_{1.875}\text{Ba}_{0.125}\text{CuO}_4$ (ref. 18). $\text{La}_{1.875}\text{Ba}_{0.125}\text{CuO}_4$ is stripe ordered with Bragg peaks corresponding to spin and charge order²⁰ and is only weakly superconducting with $T_c < 6$ K, whereas $\text{La}_{1.84}\text{Sr}_{0.16}\text{CuO}_4$ is superconducting with $T_c = 38.5$ K and has no observable spin or charge order. For a given energy, both compositions show broadly similar structures in their $\chi''(\mathbf{Q}, \omega)$ patterns. The energy dependence of the response as characterized by $\chi''(\omega)$ is very different in the two compositions. $\text{La}_{1.875}\text{Ba}_{0.125}\text{CuO}_4$ (ref. 18) shows a peak in $\chi''(\omega)$ centred on zero energy, which is probably connected to excitations owing to the magnetic order present in this compound. For $E > 15$ meV, $\chi''(\omega)$ increases to a broad maximum at about 60 meV. In contrast, in $\text{La}_{1.84}\text{Sr}_{0.16}\text{CuO}_4$, as E is increased from zero, $\chi''(\omega)$ rises from zero to a sharp maximum at 18 meV, followed by a dip at 25 meV and a second broader maximum at 50 meV. Above about 60 meV, both compositions show similar responses, with $\chi''(\omega)$ decreasing slowly with ω . The difference in the responses of the two materials below 60 meV is not surprising given that $\text{La}_{1.875}\text{Ba}_{0.125}\text{CuO}_4$ is magnetically (and charge) ordered and therefore must have excitations reflecting this ordered state.

Given the markedly different characteristics of the two components that make up the magnetic response in $\text{La}_{1.84}\text{Sr}_{0.16}\text{CuO}_4$, it is likely that they have different origins. One possible interpretation is that the lower-energy incommensurate structure is due to quasiparticle (electron-hole) pair creation, which might be calculated from an underlying band structure^{21,22}, whereas the higher-energy structure is due to the residual antiferromagnetic interactions. It is instructive to compare the magnetic response at optimal doping with that of the antiferromagnetic parent compound La_2CuO_4 (ref. 23). In La_2CuO_4 , $\chi''(\omega)$ is approximately constant over the energy range probed here (0–160 meV) with $\chi''(\omega) \approx 1.7 \mu_B^2 \text{eV}^{-1} \text{f.u.}^{-1}$. Thus, the effect of doping is to suppress the high-energy response ($\hbar\omega > 50$ meV) and enhance the response at lower frequencies, creating a double-peak structure. Figure 3c shows that the high-energy part of the response disperses with increasing energy. Constant energy cuts through the data yield two peaks (see Fig. 2) that are reminiscent of spin waves in the parent compound La_2CuO_4 . We may use the high-energy dispersion to estimate an effective Heisenberg exchange constant, J , which quantifies the strength of the coupling between the copper spins. Using the fitted values of $|\delta|$ in Fig. 3c for $E > 40$ meV, we estimate the gradient to be $dE/d\delta = 510 \pm 50 \text{ meV \AA}$. This may then be compared with the standard expression for the spin-wave velocity in a square lattice antiferromagnet, $\hbar v_s = Z_c \sqrt{8SJ}a$, where Z_c , S and a are the quantum renormalization, spin and lattice parameter respectively. We find that the effective exchange constant for $\text{La}_{1.84}\text{Sr}_{0.16}\text{CuO}_4$ is $J = 81 \pm 9 \text{ meV}$. This is substantially reduced compared with that of the parent compound La_2CuO_4 , where $J = 146 \pm 4 \text{ meV}$ (ref. 23).

We now compare our measurements of the magnetic excitations with electronic spectroscopy carried out on cuprate superconductors with the same energy scale. The energy of the 50 meV peak matches the energy range (40–70 meV) where ARPES measurements⁵ in the same compound $\text{La}_{2-x}\text{Sr}_x\text{CuO}_4$ show rapid changes or kinks in the quasiparticle dispersion $E(k)$. Theory¹⁰ has no difficulty in explaining kinks and related features around the underlying Fermi surface through coupling to spin excitations that are strongest near $(1/2, 1/2)$. In the alternative scenario where phonons are the most strongly coupled boson modes, we would expect *a priori* that there would be a series of kinks corresponding to different phonons. Coupling to the spin excitations seems to provide a more natural explanation

for the kink, because there is a single feature in the spin excitations with the required energy scale. At higher energies, ARPES measurements suggest that the quasiparticles are coupled to bosonic excitations with energies up to at least 300 meV (ref. 24). This would match the high-energy tail of the collective spin excitations in Fig. 3a. These energies are well above the phonon cutoff of about 85 meV. Other electronic spectroscopy data are not available for $\text{La}_{2-x}\text{Sr}_x\text{CuO}_4$. However, we may make comparisons with other systems. Infrared optical conductivity measurements on $\text{YBa}_2\text{Cu}_3\text{O}_{6+x}$ (ref. 25) and $\text{Bi}_2\text{Sr}_2\text{Ca}_{0.92}\text{Y}_{0.08}\text{Cu}_2\text{O}_{8+\delta}$ (ref. 26) provide evidence of coupling to high-energy bosons in the range of the 50 meV excitations reported here. The infrared optical conductivity measurements also suggest the existence of bosons at higher energies, consistent with the present experiment. It should be noted that the magnetic excitations reported here do not seem to be related to the lattice modes recently observed by scanning tunnelling microscopy²⁷ in $\text{Bi}_2\text{Sr}_2\text{CaCu}_2\text{O}_{8+\delta}$. These lattice modes are associated with the wavevector $\mathbf{q} \approx (0.2, 0)$, rather than $\mathbf{q} \approx (1/2, 1/2)$.

Received 29 August 2006; accepted 10 January 2007; published 18 February 2007.

References

1. Chubukov, A. V., Pines, D. & Schmalian, J. in *The Physics of Superconductors* Vol. 2 (eds Bennemann, K. H. & Ketterson, J. B.) 495–590 (Springer, Berlin, 2003).
2. Bogdanov, P. V. *et al.* Evidence for an energy scale for quasiparticle dispersion in $\text{Bi}_2\text{Sr}_2\text{CaCu}_2\text{O}_8$. *Phys. Rev. Lett.* **85**, 2581–2584 (2000).
3. Kaminski, A. *et al.* Renormalization of spectral line shape and dispersion below T_c in $\text{Bi}_2\text{Sr}_2\text{CaCu}_2\text{O}_{8+\delta}$. *Phys. Rev. Lett.* **86**, 1070–1073 (2001).
4. Johnson, P. D. *et al.* Doping and temperature dependence of the mass enhancement observed in the cuprate $\text{Bi}_2\text{Sr}_2\text{CaCu}_2\text{O}_{8+\delta}$. *Phys. Rev. Lett.* **87**, 177007 (2001).
5. Lanzara, A. *et al.* Evidence for ubiquitous strong electron–phonon coupling in high-temperature superconductors. *Nature* **412**, 510–514 (2001).
6. Basov, D. N. & Timusk, T. Electrodynamics of high- T_c superconductors. *Rev. Mod. Phys.* **77**, 721–779 (2005).
7. Dordevic, S. V. *et al.* Extracting the electron–boson spectral function $\alpha^2F(\omega)$ from infrared and photoemission data using inverse theory. *Phys. Rev. B* **71**, 104529 (2005).
8. McMillan, W. L. & Rowell, J. M. Lead phonon spectrum calculated from superconducting density of states. *Phys. Rev. Lett.* **14**, 108–112 (1965).

9. Stedman, R., Almqvist, L. & Nilsson, G. Phonon–frequency distributions and heat capacities of aluminum and lead. *Phys. Rev.* **162**, 549–557 (1967).
10. Chubukov, A. V. & Norman, M. R. Dispersion anomalies in cuprate superconductors. *Phys. Rev. B* **70**, 174505 (2004).
11. Shirane, G. *et al.* Temperature dependence of the magnetic excitations in $\text{La}_{1.85}\text{Sr}_{0.15}\text{CuO}_4$ ($T_c = 33$ K). *Phys. Rev. Lett.* **63**, 330–333 (1989).
12. Cheong, S. W. *et al.* Incommensurate magnetic fluctuations in $\text{La}_{2-x}\text{Sr}_x\text{CuO}_4$. *Phys. Rev. Lett.* **67**, 1791–1794 (1991).
13. Mason, T. E., Aeppli, G. & Mook, H. A. Magnetic dynamics of superconducting $\text{La}_{1.86}\text{Sr}_{0.14}\text{CuO}_4$. *Phys. Rev. Lett.* **68**, 1414–1417 (1992).
14. Christensen, N. B. *et al.* Dispersive excitations in the high-temperature superconductor $\text{La}_{2-x}\text{Sr}_x\text{CuO}_4$. *Phys. Rev. Lett.* **93**, 147002 (2004).
15. Hayden, S. M. *et al.* Comparison of the high-frequency magnetic fluctuations in insulating and superconducting $\text{La}_{2-x}\text{Sr}_x\text{CuO}_4$. *Phys. Rev. Lett.* **76**, 1344–1347 (1996).
16. Hayden, S. M., Mook, H. A., Dai, P. C., Perring, T. G. & Dogan, F. The structure of the high-energy spin excitations in a high-transition-temperature superconductor. *Nature* **429**, 531–534 (2004).
17. Stock, C. *et al.* From incommensurate to dispersive spin-fluctuations: The high-energy inelastic spectrum in superconducting $\text{YBa}_2\text{Cu}_3\text{O}_{6.5}$. *Phys. Rev. B* **71**, 024522 (2005).
18. Tranquada, J. M. *et al.* Quantum magnetic excitations from stripes in copper oxide superconductors. *Nature* **429**, 534–538 (2004).
19. Sato, H. & Maki, K. Theory of inelastic neutron scattering from Cr and its alloys near the Néel temperature. *Int. J. Magn.* **6**, 183–209 (1974).
20. Fujita, M., Goka, H., Yamada, K., Tranquada, J. M. & Regnault, L. P. Stripe order, depinning, and fluctuations in $\text{La}_{1.875}\text{Ba}_{0.125}\text{CuO}_4$ and $\text{La}_{1.875}\text{Ba}_{0.075}\text{Sr}_{0.050}\text{CuO}_4$. *Phys. Rev. B* **70**, 104517 (2004).
21. Si, Q. M., Zha, Y. Y., Levin, K. & Lu, J. P. Comparison of spin dynamics in $\text{YBa}_2\text{Cu}_3\text{O}_{7-\delta}$ and $\text{La}_{2-x}\text{Sr}_x\text{CuO}_4$ —effects of fermi-surface geometry. *Phys. Rev. B* **47**, 9055–9076 (1993).
22. Littlewood, P. B., Zaanen, J., Aeppli, G. & Monien, H. Spin fluctuations in a 2-dimensional marginal fermi-liquid. *Phys. Rev. B* **48**, 487–498 (1993).
23. Colde, R. *et al.* Spin waves and electronic interactions in La_2CuO_4 . *Phys. Rev. Lett.* **86**, 5377–5380 (2001).
24. Kordyuk, A. A. *et al.* Constituents of the quasiparticle spectrum along the nodal direction of high- T_c cuprates. *Phys. Rev. Lett.* **97**, 017002 (2006).
25. Basov, D. N. *et al.* Pseudogap and charge dynamics in CuO_2 planes in YBCO. *Phys. Rev. Lett.* **77**, 4090–4093 (1996).
26. van der Marel, D. *et al.* Quantum critical behaviour in a high- T_c superconductor. *Nature* **425**, 271–274 (2003).
27. Lee, J. *et al.* Interplay of electron-lattice interactions and superconductivity in $\text{Bi}_2\text{Sr}_2\text{CaCu}_2\text{O}_{8+\delta}$. *Nature* **442**, 546–550 (2006).

Acknowledgements

We acknowledge financial support from the EPSRC. Correspondence and requests for materials should be addressed to S.M.H. Supplementary Information accompanies this paper on www.nature.com/naturephysics.

Competing financial interests

The authors declare that they have no competing financial interests.

Reprints and permission information is available online at <http://npg.nature.com/reprintsandpermissions/>